Journal of Biomedical Optics

SPIEDigitalLibrary.org/jbo

Changes in the redox state and endogenous fluorescence of *in vivo* human skin due to intrinsic and photoaging, measured by multiphoton tomography with fluorescence lifetime imaging

Washington Y. Sanchez
Clara Obispo
Elizabeth Ryan
Jeffrey E. Grice
Michael S. Roberts

SPIE

Changes in the redox state and endogenous fluorescence of *in vivo* human skin due to intrinsic and photo-aging, measured by multiphoton tomography with fluorescence lifetime imaging

Washington Y. Sanchez,[a] Clara Obispo,[b] Elizabeth Ryan,[a] Jeffrey E. Grice,[a] and Michael S. Roberts[a,c]
[a]University of Queensland, Therapeutics Research Centre, School of Medicine, Princess Alexandra Hospital, Woolloongabba, Queensland, Australia
[b]Institut Polytechnique Lasalle-Beauvais, Department of Nutrition and Health Sciences, Beauvais, Picardie, France
[c]University of South Australia, School of Pharmacy and Medical Science, City East Campus, Adelaide, South Australia, Australia

Abstract. Ultraviolet radiation from solar exposure is a key extrinsic factor responsible for premature skin aging (i.e., photo-aging). Recent advances using *in vivo* multiphoton tomography (MPT) demonstrate the efficacy of this approach to assess intrinsic and extrinsic skin aging as an alternative to existing invasive techniques. In this study, we measured changes in epidermal autofluorescence, dermal collagen second harmonic generation (SHG), and the redox state of solar-exposed and solar-protected human skin by MPT with fluorescence lifetime imaging (MPT-FLIM). Twenty-four volunteers across four age categories (20 to 29, 30 to 39, 40 to 49, and 50 to 59 years old; six volunteers each) were recruited for MPT-FLIM imaging of the dorsal (solar-exposed; photo-damaged) and volar (solar-protected) forearm. We demonstrate a higher intensity of dermal collagen SHG within the volar forearm compared to dorsal solar-exposed skin. Redox imaging of each epidermal skin stratum by FLIM demonstrates an increase in fluorescence lifetime in the solar-exposed dorsal forearm that is more apparent in aged skin. The results of this study suggest the redox state of the viable epidermis is a key marker in assessing intrinsic and photo-damage skin aging, in combination with changes in autofluorescence and SHG. [DOI: 10.1117/1.JBO.18.6.061217]

Keywords: photo-aging; skin; redox; fluorescence lifetime imaging; photo-damage.

Paper 12619SS received Sep. 18, 2012; revised manuscript received Nov. 2, 2012; accepted for publication Nov. 2, 2012; published online Nov. 27, 2012; corrected Dec. 3, 2012.

1 Introduction

The process of human skin aging is influenced by both intrinsic and extrinsic factors. Acute and chronic ultraviolet radiation (UVR) exposure in human skin is a major extrinsic aging factor that leads to photo-aging, which is characterized by solar elastosis (elevated deposition of elastin and other extracellular matrix components in the upper dermis) and irregular and reduced collagen within the dermis.[1,2] Overall, photo-ageing leads to clinical signs of wrinkles, coarseness, formation of small blood vessels near the skin surface (telangiectasia) and irregular skin pigmentation. Acute photo-damage also causes an impairment of the barrier function of the stratum corneum, permitting greater percutaneous absorption of compounds that contact the skin.[3,4]

Photo-aging is partially mediated by UVR-induced upregulation of matrix metalloproteinases (MMPs), which degrade collagen and other matrix proteins within the dermis.[5,6] This process can be inhibited in the presence of MMP inhibitors such as tretinoin.[5] Histopathology was traditionally used to visualize changes caused by intrinsic and extrinsic aging within the dermis. While straightforward and well characterized, this "invasive" approach requires an excised skin biopsy from patients. This is a key obstacle for larger population studies and painful for individual patients.[2]

Noninvasive high resolution imaging, such as multiphoton tomography (MPT), has emerged as a viable alternative to histopathology to assess both intrinsic and photo-aging of human skin in real-time and *in vivo*.[1,2] MPT involves two-photon excitation of endogenous autofluorescent compounds within the epidermis, such as nicotinamide adenine dinucleotide (NADH), the NADH phosphate derivative (NADPH) and flavin adenine dinucleotide (FAD). Matrix components within the dermis, such as collagen, are visualized by MPT via an optically nonlinear phenomenon known as second harmonic generation (SHG).[1,7]

MPT has been used extensively to visualize and quantify the extent of photo-aging by measuring the distribution and quantity of matrix proteins, predominantly collagen, within the upper dermis of the skin.[1,2,8] Photo-aging is quantified by MPT imaging by measuring the SHG to autofluorescence ageing index of dermis (SAAID), which uses the tendency of autofluorescence to increase and collagen SHG to decrease with photo-aging in the superficial layer of the dermis.[5,6,9,10] Photo-aging can also be assessed with MPT by measuring ratio of elastin autofluorescence to collagen SHG.[5,11] Changes in keratinocyte morphology and epidermal thickness can be assessed by MPT.[2,12,13]

Photo-damage and premature aging of the skin is not limited to structural changes of matrix proteins within the dermis. UVR

Address all correspondence to: Michael S. Roberts, The University of Queensland, Therapeutics Research Centre, School of Medicine, Princess Alexandra Hospital, Woolloongabba, Queensland, Australia. Tel: +617 3176 2637; Fax: +617 3176 5806; E-mail: m.roberts@uq.edu.au

0091-3286/2012/$25.00

exposure in the skin leads to profound changes in the metabolic state of epidermal cells, including oxidative stress from an increase in the generation of reactive oxygen species[1,2,14,15] and the inhibition of free fatty acid synthesis.[1,7,16] Metabolic changes are associated with alterations in the redox state of the cell, which can be measured noninvasively using MPT in combination with fluorescence lifetime imaging (FLIM).[7,17] FLIM constructs an image based on the fluorescence decay rates of one or more fluorescent molecules within a sample, following a time-resolved analysis of a fluorescence signal after excitation.[17] Both NAD(P)H and FAD are robust metabolic, redox and cell death indicators using MPT-FLIM.[18–20]

The aim of this study was to characterize changes associated with intrinsic factors and photo-aging in the structural, functional, and metabolic state of *in vivo* human skin. We used MPT-FLIM to examine changes in the endogenous autofluorescence (AF) and redox state of the epidermis and collagen SHG in the dermis, in dorsal (solar-exposed) and volar (solar-protected) forearm skin of volunteers of various ages. We also examined differences in the penetration of topically applied fluorescent dyes to solar-exposed and solar-protected forearm skin.

2 Materials and Methods

2.1 *Volunteers*

Characterization of intrinsic and photo-aging by MPT-FLIM was conducted in accordance with approval of Princess Alexandra Hospital Research Committee Approval No. 2008001342, which is administered by the University of Queensland Human Ethics Committee. Our study involved a total of 24 healthy subjects divided into four age groups: 20 to 29, 30 to 39, 40 to 49, and 50 to 59 years old. MPT-FLIM images were taken at two sites: the dorsal (solar-exposed, photo-damaged) and volar (solar-protected) mid-forearm. Each group contained three male and three female subjects with undamaged skin and no history of cutaneous disease. Consent was obtained after informing the volunteers about the imaging details.

2.2 *MPT-FLIM Imaging*

MPT of volunteer skin was carried out using the DermaInspect® system (JenLab GmbH, Jena, Germany). Source excitation light was provided by an ultra-short pulsed, mode-locked (80-MHz) femtosecond titanium sapphire laser (Mai Tai, Spectra Physics, Mount View, California), with an 85 fs pulse width and tuning range of 710 to 920 nm. All images were taken using a Plan-Neofluar high-NA oil-immersion $40\times/1.30$ objective lens (Carl Zeiss, Germany). Using a constant incident optical power of 31 mW, endogenous cellular autofluorescence was imaged at an excitation laser wavelength of 740 nm (two-photon) while collagen SHG was imaged using an excitation wavelength of 800 nm. Autofluorescence emission and SHG signals were measured with a 350 to 650 nm broad-bandpass filter (BG39, Schott glass color filter, Schott MG, Mainz, Germany). Each image was 179×179 μm wide, taken with a scan time of 4.35 s at a resolution of 512×512 pixels.

For FLIM measurements, a time-correlated single-photon counting (TCSPC) SPC-830 detector (Becker & Hickl GmbH, Berlin, Germany) was integrated into the MPT system. The TCSPC module constructs a photon distribution across the x and y coordinates of the scan area. For each photon detected, the module determines the time of arrival within the fluorescence decay. In front of the FLIM detectors, a 350 to 650 nm broad-bandpass filter (BG39, Schott glass color filter) was used to filter the emitted light. Each FLIM scan was performed using an exposure of 13.4 s at an acquisition image size of 214×214 μm^2. For each image site on the dorsal and ventral forearm, FLIM images were taken at three depths: 5 to 10, 20 to 30 and 40 to 50 μm from the SC, corresponding to the three layers of the epidermis [stratum granulosum (SG) and stratum spinosum (SS) and stratum basale (SB)]. The correct layer was also confirmed by keratinocyte morphology.

2.3 *Autofluorescence and SHG Intensity Versus Skin Depth and Epidermal Thickness*

One hundred twenty Z-stack images were taken starting from the stratum corneum (SC) surface at a spacing of 2 μm using 740 and 800 nm excitation wavelengths. Using the ImageJ application (http://rsbweb.nih.gov/ij/), a region of interest (ROI) was drawn to encompass epidermal cells through the Z-stack and measure the ROI area and integrated density. The background fluorescence intensity (FI) was also measured from six blank regions. The normalized FI within the ROI for each Z-stack image was calculated according to:

$$\text{Norm.FI} = \text{ROI}\left(\frac{\text{Integrated density}}{\text{Area}}\right) - \text{Background}\left(\frac{\text{Integrated density}}{\text{Area}}\right). \quad (1)$$

2.4 *SAAID*

The SHG to autofluorescence aging index (SAAID) was calculated as described previously.[9] Both SHG signal (800 nm) and autofluorescence (AF; 740 nm) intensity was measured using MPT images taken from a gated area $\sim177\times172$ μm at a depth of 40 μm below the epidermal-dermal junction. The following formula was used to calculate SAAID:

$$\text{SAAID} = \frac{\text{SHG} - \text{AF}}{\text{SHG} + \text{AF}}. \quad (2)$$

2.5 *FLIM Data Analysis*

FLIM data was analyzed using SPCImage 3.8.9 software (Becker & Hickl GmbH, Berlin, Germany) to generate fluorescence lifetime and photon contribution histograms. This data can be considered as an array of pixels that contains many time channels distributed across the fluorescence decay, with each pixel possessing a decay curve. The decay curve is a sum of several exponentials as each pixel represents an overlay of emissions from various endogenous fluorophores (that may or may not be found in the same photo-physical state). For our study, the decay curve was fitted using a double-exponential decay model function[1]:

$$f(t) = \alpha_1 e^{\frac{-t}{\tau_1}} + \alpha_2 e^{\frac{-t}{\tau_2}} \quad \text{with } \alpha_1 + \alpha_2 = 1. \quad (3)$$

This fitted decay curve produces two lifetimes: the short (τ_1) and long (τ_2) fluorescence lifetimes (ps) along with corresponding relative amplitude coefficients α_1 and α_2 (%).

The instrument response function (IRF) was calibrated to a sucrose crystal standard (Ajax Finechem Pty. Ltd., Sydney,

NSW, Australia). For each FLIM image, the IRF(t) is convoluted with the model function, $f(t)$, to generate the function $F(t)$. This function corresponds to the shape of the signal if the measured optical signal was the same as the model function $f(t)$.

$$F(t) = f(t) * \mathrm{IRF}(T), \tag{4}$$

where * represents the convolution symbol. The $F(t)$ function is fitted to each measured data point to calculate the necessary decay parameters and create both a pseudo-color image and histogram of the average weight lifetime τ_m, which is the weighted average lifetime calculated from τ_1 and τ_2 and their relative amplitudes (i.e., % contribution of τ_1 and τ_2 lifetimes in a pixel). The τ_m pixel frequency data, of a defined region of interest within each scan (i.e., gating for visible keratinocytes within the SG and SS) was exported using SPCImage. The data was normalized according to the area of the region of interest and used to calculate the mean τ_m lifetime distribution histograms. τ_m lifetime data was collected from two emission spectral channels: NAD(P)H (350 to 450 nm) and NAD(P)H/FAD (450 to 515 nm). Redox images of each epidermal layer (SG, SS and SB) were pseudo-colored according to the average weighted lifetime (τ_m; 0 to 2000 ps).

2.6 *Topical Staining of Solar-Exposed and Solar-Protected In Vivo Skin*

For topical staining of the skin, we applied 20 μl of a 10 μM solution of acriflavine (52 ng/cm^2; Sigma-Aldrich Pty. Ltd, Castle Hill, NSW, Australia) and/or 6-carboxyfluorescein (6-CF; 75 ng/cm^2; Sigma-Aldrich Pty. Ltd.) in PBS to a 1 cm^2 area on the skin surface of the dorsal (solar-exposed) and volar (solar-protected) forearms of volunteers aged 20 to 29 ($n = 3$) and 50 to 59 years old ($n = 3$). After 1 h, the staining area on the skin was wiped with a lint-free tissue paper and imaged by MPT-FLIM at an excitation wavelength of 740 nm (2-photon) within the SG (~5 to 10 μm beneath the SC and morphologically validated). Fluorescence emission was collected and analyzed by a third TCSPC FLIM detector through a broad bandpass filter (515 to 620 nm) to measure changes in the average τ_m fluorescence lifetime of the viable epidermis due to the presence of acriflavine and/or 6-CF. The pixel intensity (pixel frequency multiplied by the photon count) was normalized to the area of the region of interest, gated using SPCImage. FLIM images of the SG were pseudo-coloured according to the average weighted lifetime (τ_m; 0 to 5000 ps).

2.7 *Statistical Analysis*

Data is expressed as mean ± standard error of the mean (SEM) ($n = 6$). Statistical comparison of the average lifetime, epidermal thickness or SAAID between solar-exposed and protected forearms, within each age group and epidermal layer, was made using Wilcoxon matched-pairs signed rank test. Statistical differences within an epidermal layer, of either the solar-exposed or protected forearm, across the age groups was determined using a one-way ANOVA with a post-hoc Tukey's test. To assess differences in the average lifetime, epidermal thickness or SAAID due to intrinsic aging and photo-damage simultaneously, a repeated measures two-way ANOVA was performed with a Bonferroni's post-test. All the statistical analysis was done using GraphPad Prism v5.03 (GraphPad Software Inc., La Jolla, California). A p value of less than 0.05 was considered to be statistically significant.

3 Results

3.1 *Change in Epidermal AF and Dermal Collagen SHG Intensity with Skin Depth*

Figure 1 shows representative AF and SHG images within the stratum corneum (SC), granulosum (SG), spinosum (SS), basale (SB) and upper dermis of volar and dorsal forearm from a subject of the 30 through 39 years old group. The images show a marked reduction of collagen observed within the dermis in the dorsal (solar-exposed) forearm compared to the volar (solar-protected) side.

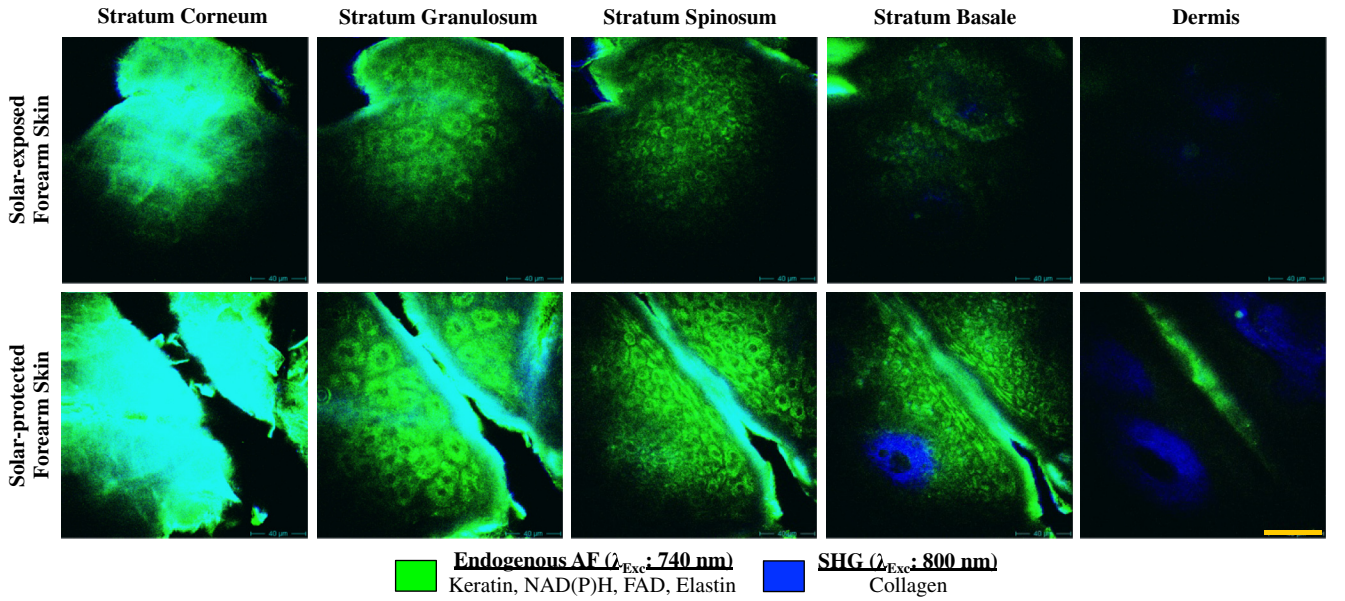

Fig. 1 Representative multiphoton images of the dorsal (solar-exposed) and volar (solar-protected) forearm skin (male subject aged 20 to 29 years old). Images are an overlay of the fluorescence emission (350 to 450 nm) at an excitation of 740 (green) and 800 nm (blue) to capture endogenous AF and collagen SHG, respectively. The yellow scale bar indicates a length of 40 μm.

The AF intensity was comparable between volar and dorsal forearms for individuals of all age categories [Fig. 2(a)]. For all age groups there was a tendency for reduced collagen SHG within the dermis of the dorsal forearm [Fig. 2(a)]. At a depth of 60 μm from the SG, the collagen SHG signal in the solar-protected forearm was significantly ($p < 0.05$) higher than the solar-exposed forearm.

Figure 2(b) demonstrates that for either the solar-exposed or protected forearm, the AF and SHG signal tended to be higher for subjects aged between 50 and 59 years old than for other age groups. However, these differences were not statistically significant.

3.2 *SAAID and Epidermal Thickness*

The SAAID parameters for solar-exposed skin—at a depth of 40 μm below the epidermal-dermal junction—for the 20 to 29, 30 to 39, 40 to 49, and 50 to 59 year old age groups were 0.07 ± 0.04 au, 0.03 ± 0.03 au, 0.17 ± 0.06 au and 0.06 ± 0.08 au, respectively [Fig. 3(a)]. For solar-protected skin, the SAAID values were 0.23 ± 0.07 au, 0.20 ± 0.11 au, 0.23 ± 0.09 au and 0.26 ± 0.08 au, respectively. Figure 3(a) shows that the SAAID index was significantly lower in solar-exposed forearm of 20 to 29 year old subjects than solar-protected skin. For each respective age group, the SAAID index in solar-exposed skin trended lower than solar-protected skin, but significant differences were only seen for 20 to 29 year old subjects. The tendency for the SAAID intensity to be lower in the forearms of solar-exposed volunteers, across all age groups, was statistically significant ($p < 0.05$). The SAAID index for either solar-exposed or protected skin did not appear to change with age [Fig. 3(a)].

Figure 3(b) indicates that there was no significant difference in the epidermal thickness of solar-exposed versus protected

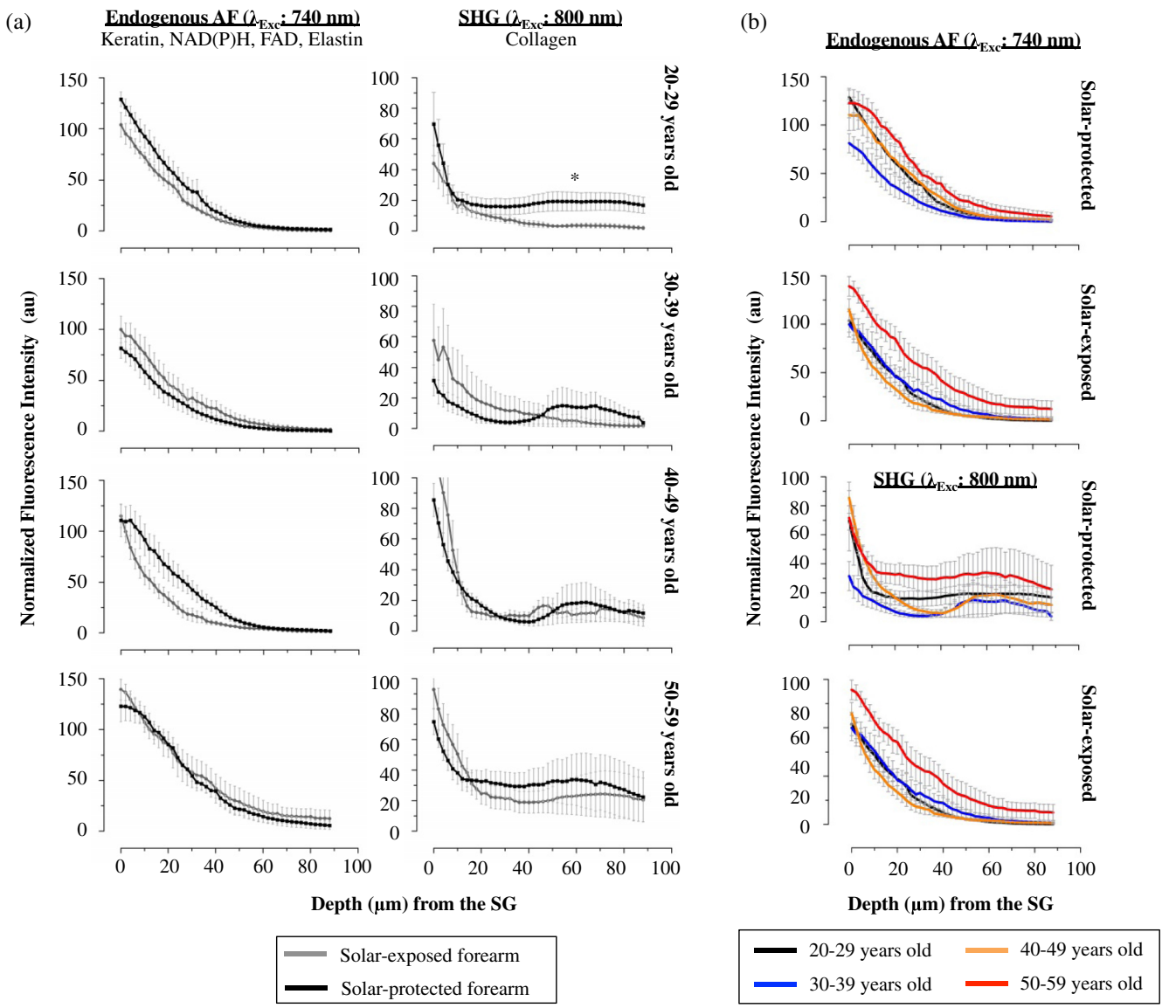

Fig. 2 Autofluorescence and SHG intensity curve of the viable epidermis and dermis. (a) In each group (20 to 29, 30 to 39, 40 to 49 and 50 to 59 years old), the normalized fluorescence intensity was measured after excitation at 740 and 800 nm (2-photon) in solar-exposed (grey) and solar-protected (black) forearm skin. (b) The autofluorescence and SHG intensity curves of 20 to 29 (black), 30 to 39 (blue), 40 to 49 (orange) and 50 to 59 (red) year old subjects are compared within solar-exposed or solar-protected groups. Error bars represent the SEM of the average normalized fluorescence intensity ($n = 5$ to 6/forearm side/age group). Significant differences are indicated with an asterisk (* for $p < 0.05$).

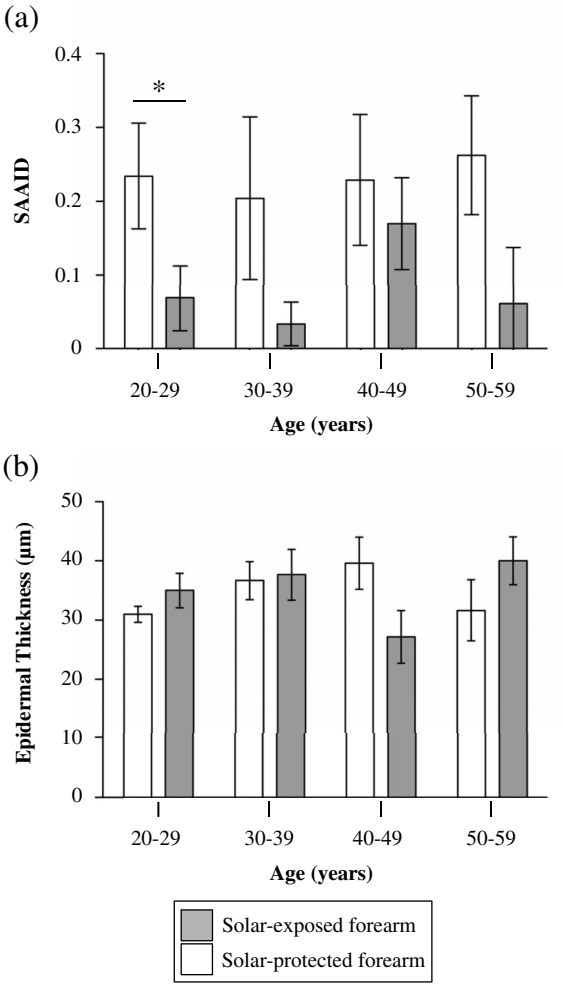

Fig. 3 SAAID (a) aging index and epidermal thickness (b) values of solar-exposed (gray) and solar-protected (white) forearm skin of each indicated age group. Error bars represent the SEM of the average SAAID or epidermal thickness ($n = 5$ to 6/forearm side/age group). Significant differences are marked by an asterisk (* for $p < 0.05$).

skin for volunteers aged 20 through 29 (35 ± 2.91 versus 31 ± 1.34 mm), 30 through 39 (37.67 ± 4.27 versus 36.67 ± 3.17 mm), 40 through 49 (27.2 ± 4.45 versus 39.6 ± 4.4 mm) and 50 through 59 (40 ± 4.07 versus 31.7 ± 5.15 mm) years old, respectively. Similarly, there was no significant change in the epidermal thickness with age.

3.3 *Redox Imaging of Sun-Protected and Exposed In Vivo Skin*

Figure 4 shows representative redox images from solar-protected and exposed forearm skin of each age category. Figure 5(a) and 5(b) chart the average weighted lifetime histograms from all the volunteers, comparing solar-protected and exposed forearm skin for each skin stratum and age group.

We observed a significant increase ($p < 0.05$) in the average τ_m lifetime of NAD(P)H in the SG of the solar-protected forearm (832.1 ± 94.7 ps) compared to the solar-exposed forearm (682 ± 96.4 ps) of 20 to 29 year old subjects [Fig. 5(a)]. Within the SB, the average lifetime was significantly higher in the solar-protected forearm versus solar-exposed skin of 40 to 49 (1005 ± 81.7 versus 521.7 ± 72.9 ps respectively) and 50 to 59 (656.6 ± 42.9 versus 596.9 ± 57.2 ps respectively) year old subjects. Similarly, the average lifetime of NAD(P)H/FAD was significantly higher in solar-protected skin (1257 ± 70.7 ps) than solar-exposed skin (826.5 ± 98.8 ps) for 40 to 49 year old subjects.

Overall, we observed a statistically significant ($p < 0.05$) tendency for average τ_m lifetime of NAD(P)H [Fig. 5(a)] and NAD(P)H/FAD [Fig. 5(b)] to be elevated within each epidermal stratum for solar protected skin versus solar-exposed skin, in each age group. This indicates photo-damage may be responsible for a redox difference observed between solar-exposed and solar-protected skin.

We observed NAD(P)H lifetime changes due to intrinsic aging within the solar-protected forearm in all of the epidermal layers [Fig. 5(a)]. In the SG, the average NAD(P)H lifetime for solar-exposed skin from 20 to 29 year old subjects (682 ± 96.4 ps) was significantly lower than for 50 to 59 year old subjects (994.6 ± 71.5 ps). In the SS, the average NAD(P)H lifetime of the solar-protected forearm skin from 20 to 29 year old volunteers (789.3 ± 57.9 ps) was significantly lower ($p < 0.05$) than subjects aged 40 to 49 (1114 ± 91.1 ps).

For the SB, the average NAD(P)H lifetime of solar-protected forearm skin from 20 to 29 year old subjects (576.5 ± 78.8 ps) was significantly lower ($p < 0.01$) than the average NAD(P)H lifetime 40 to 49 year olds (1005 ± 81.7 ps). However, the average NAD(P)H lifetime of solar-protected forearm skin from 40 to 49 year olds was significantly ($p < 0.05$) higher than 50 to 59 year olds (654.4 ± 52.5 ps).

In the solar-exposed forearm, the average τ_m NAD(P)H lifetime within the SG was significantly lower ($p < 0.05$) in 20 to 29 year olds (536.6 ± 54 ps) compared to 30 to 39 year old subjects (808.7 ± 115 ps), which was also significantly higher ($p < 0.05$) than the age-related change in the average τ_m NAD(P)H lifetime of 40 to 49 year olds (521.7 ± 72.9 ps). The only statistically significant age-related difference in the τ_m NAD(P)H/FAD lifetime was observed in the SG of solar-exposed forearm skin where the average lifetime for 20 to 29 year olds (991.1 ± 98.5 ps) was lower than that of 30 to 39 year old subjects (1263 ± 65.9 ps) [Fig. 5(b)].

Collectively, these data demonstrate an increase in the average weighted lifetime of solar-protected skin compared to solar-exposed skin, suggesting a redox change associated with solar exposure and photo-damage. We also observed an increase in the average lifetime of NAD(P)H associated with intrinsic aging, predominantly within solar-protected skin.

In Fig. 6, we further examined the lifetime (τ_1 and τ_2) and amplitude coefficient (α_1) differences between the solar-exposed and solar-protected forearm of a representative subject aged 40 through 49 years old. Figure 6(a) shows FLIM images of the SG and SB, of the solar-exposed and solar-protected forearm, pseudo-colored for the short (τ_1) and long (τ_2) NAD(P)H lifetimes and τ_1 amplitude coefficient (α_1). The FLIM images of the solar-protected side of the forearm, of both the SG and SB, appeared brighter than the solar-exposed side [Fig. 6(a)].

The τ_1 (287.6 ps) and τ_2 (2269.9 ps) lifetimes of the solar-exposed SG displayed a lower lifetime shift relative to the solar-protected SG (481.6 and 2644.6 ps, respectively) (Fig. 6). Similarly, the solar-exposed SB τ_1 (107.5 ps) and τ_2 (1847.5 ps) lifetimes were lower than the solar-protected SB (605.8 and 2810.1 ps, respectively). In contrast, the solar-exposed α_1 values

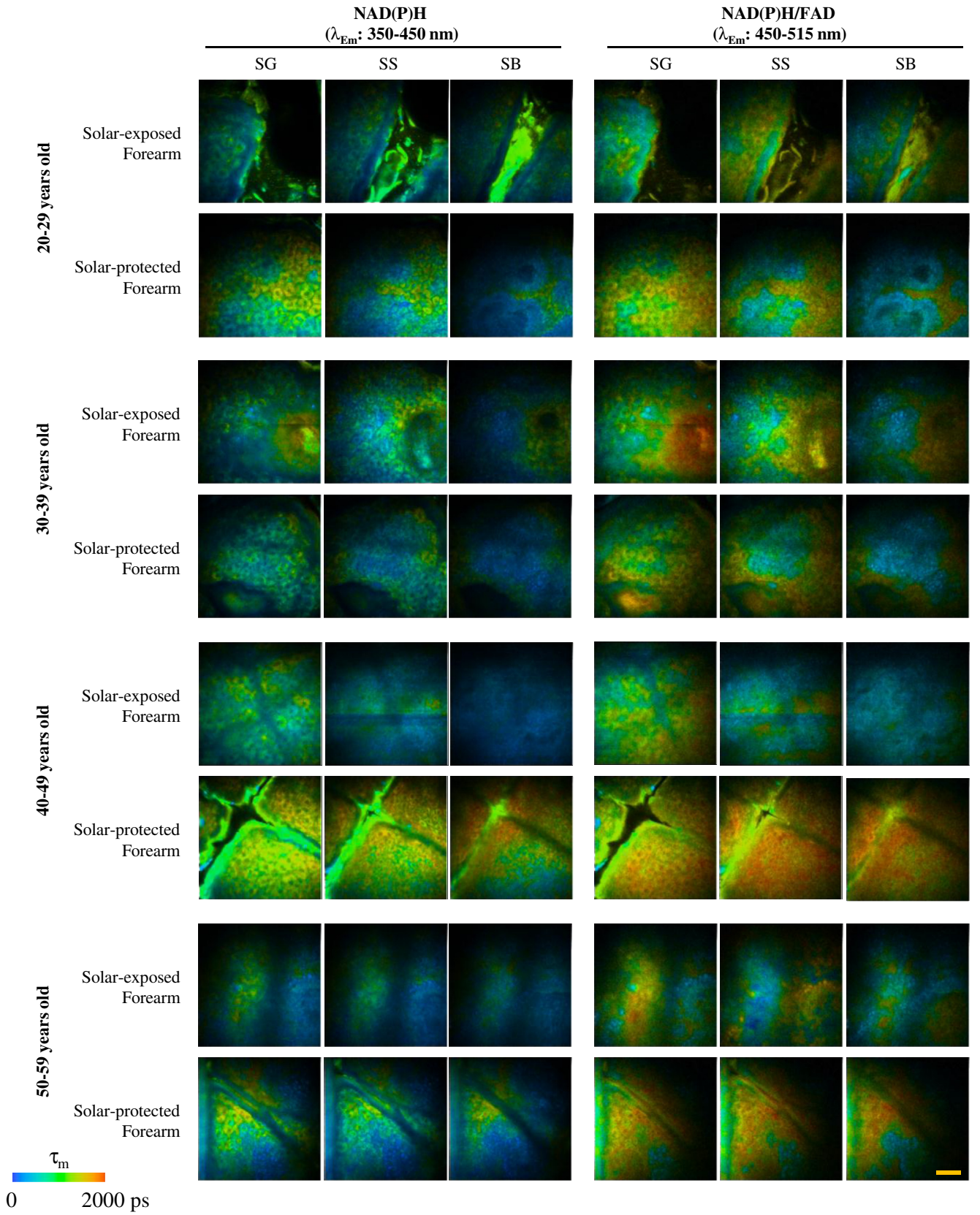

Fig. 4 Representative MPT-FLIM images of the viable epidermis (SG, SS and SB) within solar-exposed and solar-protected forearm skin of each indicated age group. FLIM images were measured within a spectral range of 350 to 450 and 450 to 515 nm to capture NAD(P)H and NAD(P)H/FAD, respectively. Redox images were pseudo-colored according to the average-weighted fluorescence lifetime (τ_m) within a range of 0 to 2000 ps (blue-to-red). Each image is $214 \times 214 \times 1$ μm^3. Scale bars (yellow) indicate a length of 40 μm.

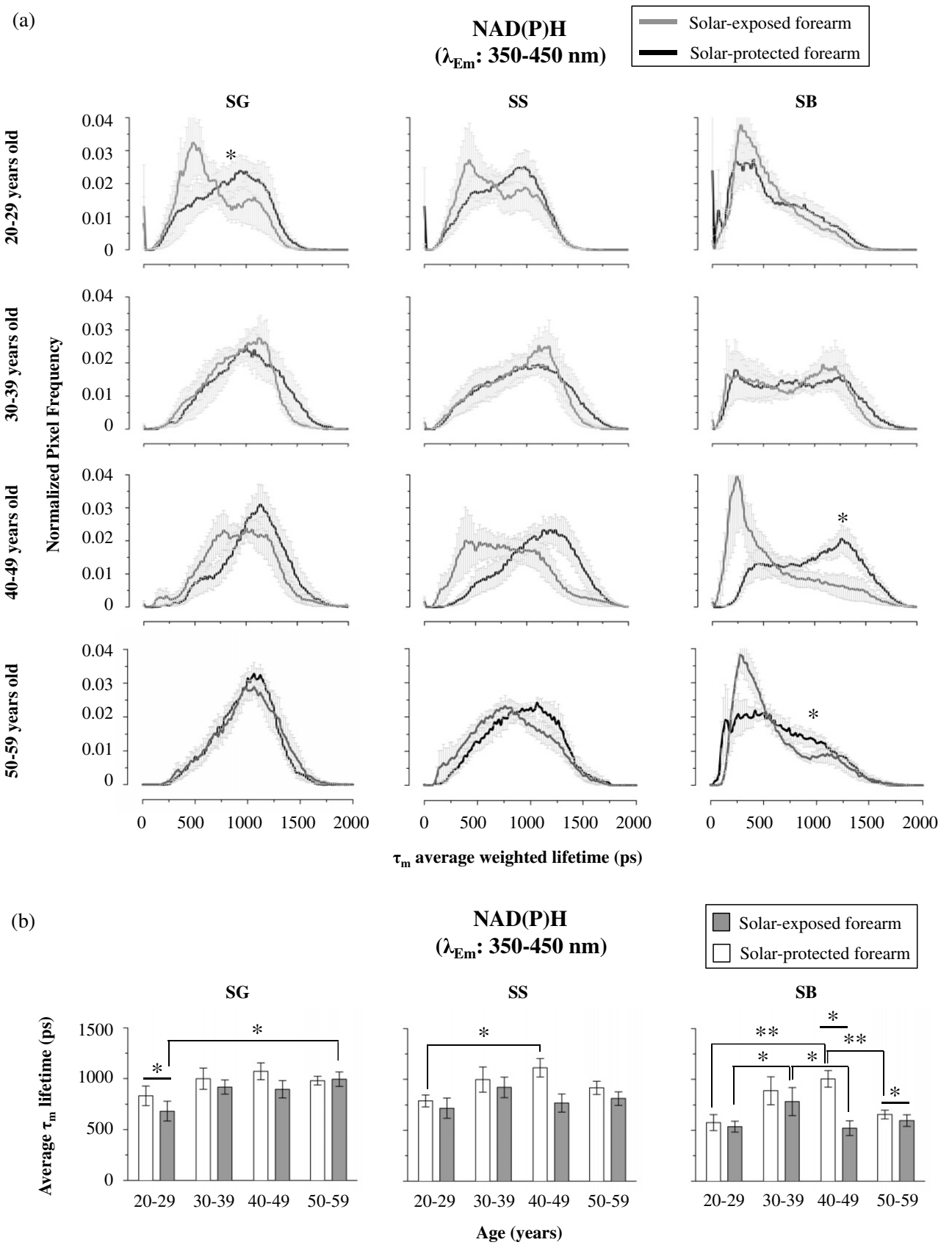

Fig. 5 τ_m lifetime histograms of NAD(P)H (a) and NAD(P)H/FAD (c) within the viable epidermis (SG, SS and SB) of solar-exposed and solar-protected forearm skin of each indicated age group. The histogram represents the average normalized pixel frequencies for each τ_m lifetime within the gated ROI, encompassing viable epidermal cells. The corresponding average τ_m lifetime of NAD(P)H (b) and NAD(P)H/FAD (d), for solar-exposed and solar-protected skin, is charted for each age group. Error bars representing the SEM ($n = 6$/forearm side/age group), with significant differences marked by an asterisk (* $p < 0.05$, ** $p < 0.01$).

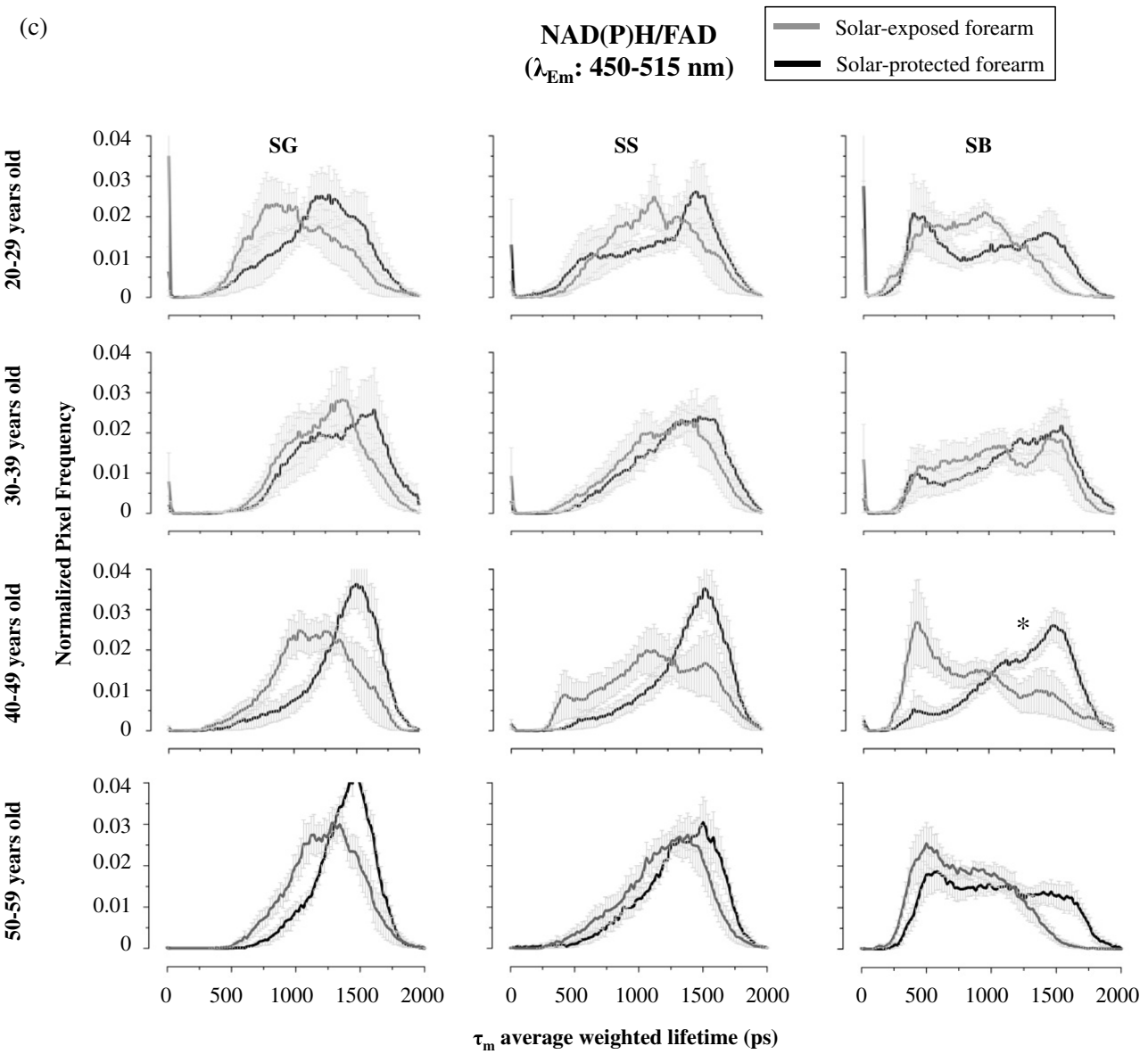

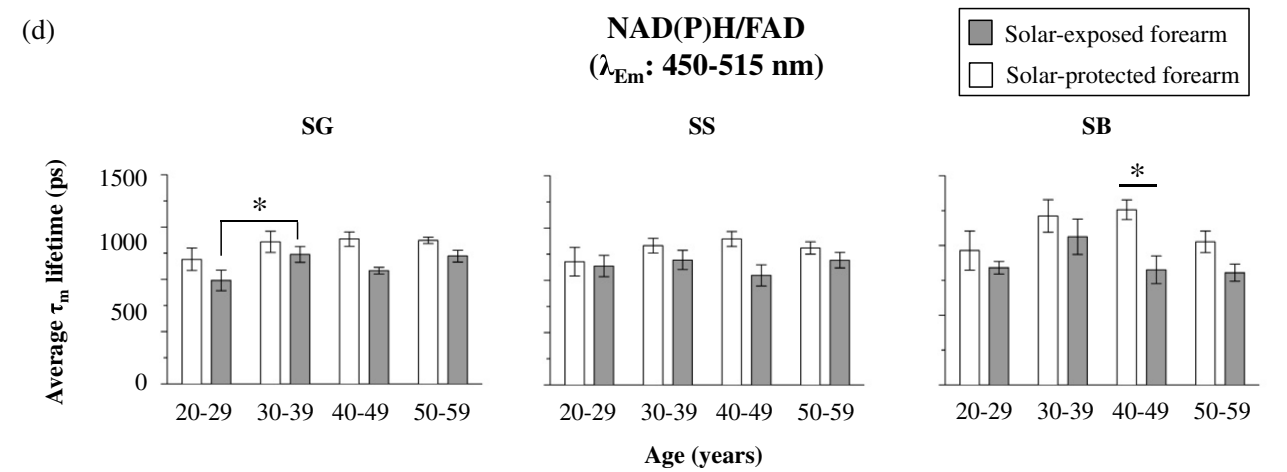

Fig. 5 (*Continued.*)

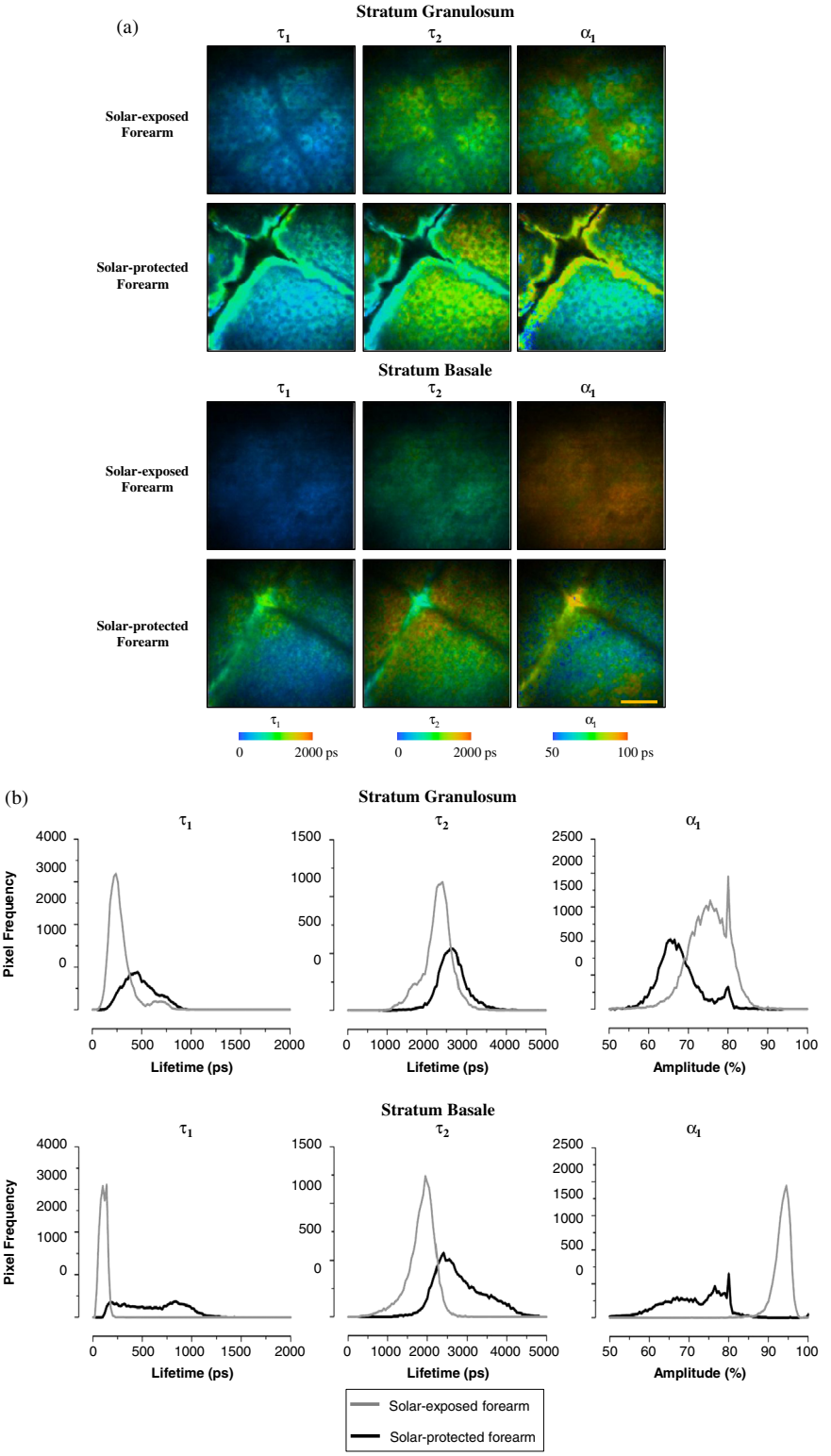

Fig. 6 Representative τ_1, τ_2 and α_1 FLIM images (a) and histograms (b) of solar-exposed (gray) and solar-protected (red) forearm skin (SG and SB) of a subject aged 40 to 49 years old. (a) FLIM images were pseudo-colored (blue-to-red) according to τ_1 (0 to 2000 ps), τ_2 (0 to 2000 ps) and α_1 (50 to 100%) parameters. (b) Histograms display the pixel frequencies for each FLIM parameter within the gated ROI, encompassing viable epidermal cells.

of the SG (75%) and SB (93.5%) displayed a red shift relative to the solar-protected skin (67.7% and 71.6%, respectively) [Fig. 6(b)]. This data suggests that the lower average lifetime of solar-exposed skin (Fig. 5) is due to both shorter τ_1 and τ_2 lifetimes as well as an increase in the τ_1 component compared to solar-protected skin.

3.4 *Fluorescent Staining of Intrinsically Aged and Photo-Aged Skin*

Figure 7(a) shows representative τ_m FLIM images (λ_{Em}: 515 to 620 nm) of the solar-protected forearm skin (SG) of a subject aged 20 to 29 years old after the topical application of

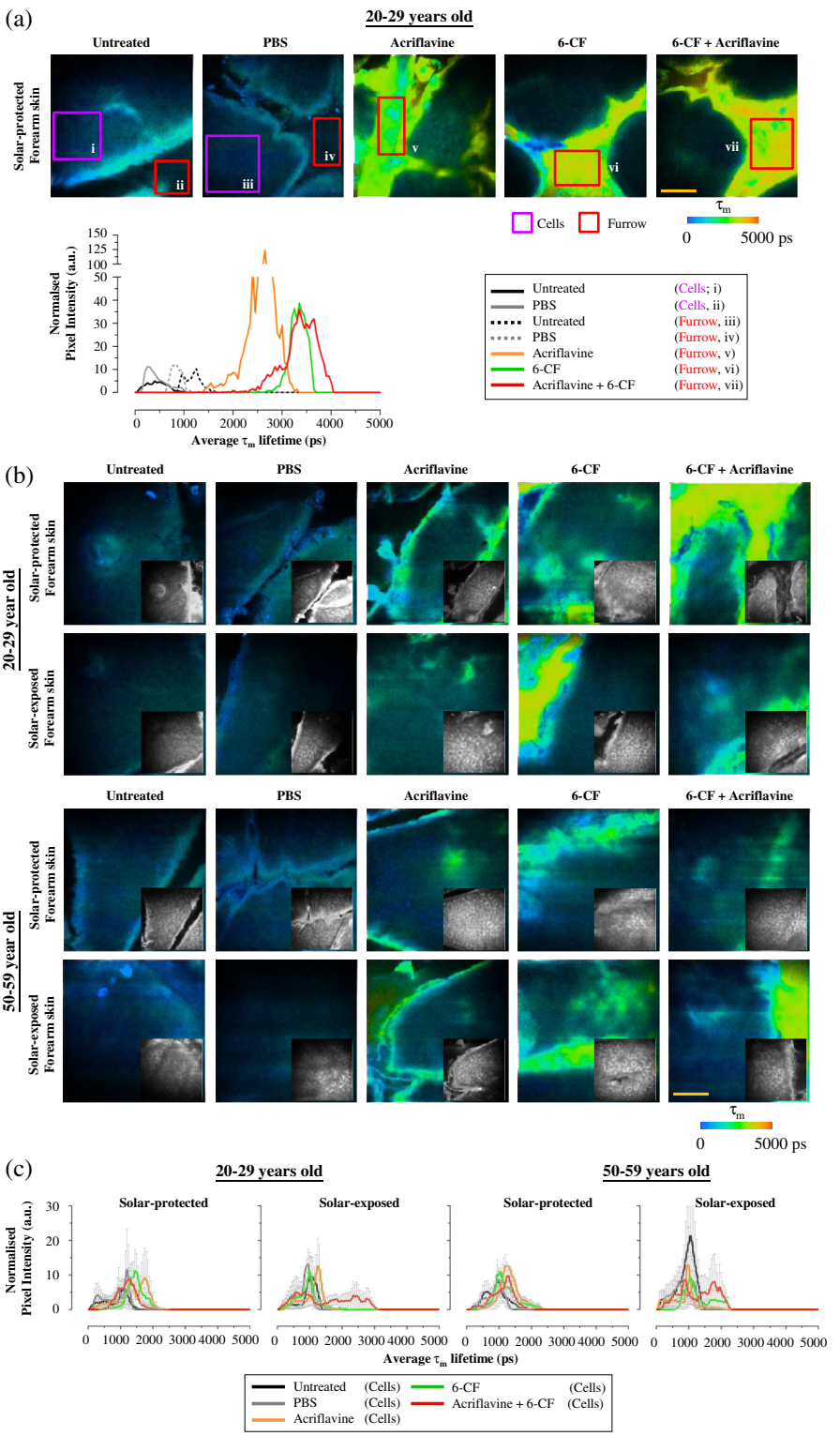

Fig. 7 Representative τ_m lifetime FLIM images (a) of solar-protected skin (SG) after staining with acriflavine and/or 6-CF, along with negative and vehicle controls. The cellular and furrow ROI are indicated by the purple and red boxes, respectively. Normalized pixel intensities of the τ_m lifetimes are plotted for either the cellular or furrow ROI of each treatment: untreated control (black; cells [i]: continuous line, furrow [ii]: hashed line), PBS (vehicle control; gray; cells [iii]: continuous line, furrow [iv]: hashed line), acriflavine (orange [v]), 6-CF (green [vi]) and acriflavine + 6-CF (red [vii]). (b) Representative τ_m lifetime FLIM images of solar-exposed and solar-protected forearm skin (SG), 1 h following the topical application of acriflavine (52 ng/cm^2) and/or 6-CF (75 ng/cm^2) along with negative and vehicle (PBS) controls. FLIM data were measured within a spectral range of 515 to 620 nm and pseudo-colored (blue-to-red) according to a τ_m lifetime range of 0 to 5000 ps. Viable epidermal cells can be observed within the corresponding grayscaled images (λ_{Em}: 350 to 450 nm) displayed in the bottom right corner of each FLIM image. (c) The average τ_m lifetime histograms of the solar-exposed and solar-protected forearm skin (SG) from subjects aged 20 to 29 and 50 to 59 years old. Normalized pixel intensities of the τ_m lifetimes are plotted for the cellular ROI of each treatment: untreated control (black), PBS (vehicle control; gray), acriflavine (orange), 6-CF (green) and acriflavine + 6-CF (red). The error bars indicate the SEM (n = 3/forearm side/age group).

acriflavine (52 ng/cm^2) and/or 6-CF (75 ng/cm^2). The τ_m histograms of the untreated and vehicle controls, within the viable epidermal cells and furrows (Fig. 7(a), i though iv), display τ_m lifetimes ranging between 0 and 1500 ps. After topical application, both acriflavine and 6-CF were predominantly localized within the furrow, with τ_m lifetimes between ~2000 to 3000 and ~3000 to 3500 ps, respectively. Acriflavine, in combination with 6-CF, also localized within the furrow, showing a τ_m lifetime between ~3000 to 4000 ps [Fig. 7(a)].

Figure 7(b) shows representative FLIM τ_m images (λ_{Em}: 515 to 620 nm) of solar-exposed and solar-protected forearm skin (SG), from volunteers aged 20 to 29 ($n = 3$) and 50 to 59 years old ($n = 3$), stained with acriflavine and/or 6-CF. The data demonstrates that there were no apparent differences in the staining of viable epidermal cells, within the SG, between intrinsically aged or photo-damaged skin after the topical application of these vital dyes [Fig. 7(b)]. Figure 7(c) demonstrates that the τ_m lifetime histograms of the viable epidermis cells largely overlap with the negative and vehicle controls (~0 to 1500 ps). Despite the observation of some lifetimes >2000 ps in solar-exposed skin for both age groups, the lifetime histograms do not correspond with acriflavine and/or 6-CF lifetimes measured within the furrow [Fig. 7(a)], suggesting minimal penetration of the dyes into the SG. This data indicates that the topical application of acriflavine and 6-CF dyes was unable to reveal any impaired barrier protection associated with photo-aging.

4 Discussion

In this study, we demonstrate the synthesis of a number of optical techniques to measure changes associated with intrinsic aging and photo-aging. By examining the endogenous AF and collagen SHG signal intensity, we observe reduced collagen SHG levels in the dermis of the volar forearm. As expected, these changes are reflected in the SAAID dermal aging index. FLIM analysis of the SG, SS and SB layers of the epidermis demonstrates several lifetime changes that are associated with intrinsic aging and photo-aging, which are discussed below.

Within the dermis, the endogenous AF signal intensity is reported to increase with aging due to the increased deposition of elastin, while collagen SHG intensity is reduced.[9] This tendency is used as the basis of the SAAID index for quantifying dermal intrinsic and photo-aging. However, this approach measures differences in the SAAID index at a single depth within the dermis and not potential changes in the endogenous AF of the epidermis. Epidermal AF, predominantly due to NAD(P)H and FAD, is a metabolic indicator of redox changes due to ischemic necrosis, oxidative stress and cell death.[18,19,21–23]

In our study, we demonstrate a tendency for epidermal AF to be elevated for subjects aged 50 through 59 years old compared to the other age groups, particularly for the solar-exposed forearm [Fig. 2(b)]. As expected, this trend continued well into the dermis, corresponding to elevated elastin in photo-aged skin.[9,24] Elevated NADH autofluorescence is typically associated with hypoxic injury and the early stages of ischemic necrosis.[18,25]

Several studies have shown the efficacy of using the SAAID index to quantify the state of intrinsic aging and photo-aging in *in vivo* human skin. Lin et al. was the first to demonstrate a decrease in the SAAID index with aging, via MPT, in solar-exposed facial skin samples.[9] A follow-up study showed that a decrease in the SAAID index is associated with intrinsic aging.[26] When comparing the SAAID index between the solar-exposed (dorsal) and protected (volar) forearms, the index was found to be higher in the solar-protected forearm of older volunteers only.[27]

In contrast, our study only found significant differences in the SAAID index between solar-exposed and protected skin for volunteers aged between 20 and 29 years old. This is associated with a clear difference in the collagen SHG intensity between solar-exposed and protected skin for this age group [Fig. 3(a)]. While there was a tendency for the SAAID index to be lower in the other age groups, these differences were not statistically significant. Robust differences may be seen by increasing the number of volunteers for this type of study, as demonstrated previously.[10] Despite this, when comparing the SAAID index of solar-exposed to solar-protected skin for all age groups, the index was significantly lower. This result agrees with a previous study showing lower SAAID indices in photo-damaged skin compared to solar-protected skin.[27]

We found no significant differences in the epidermal thickness between solar-exposed and protected skin of any age group [Fig. 3(b)]. Likewise, there was no significant change in epidermal thickness with age. These results are consistent with a previous study measuring epidermal thickness by MPT in the forearms of young, middle-aged and old volunteers.[12] To our knowledge, this is the first study to examine potential differences in the epidermal thickness between solar-exposed and solar-protected skin. To date, epidermal thickening due to photo-aging, or a decrease in thickening from intrinsic ageing,[28] has not been resolved by MPT and further studies are required to optimize this approach to observe and quantify these changes.

Our data shows a significant increase in the fluorescence lifetime of NAD(P)H in the stratum granulosum of 50 through 59 year old solar-exposed skin compared to 20 through 29 year old subjects (Figs. 4 and 5). This data is consistent with a previous study examining keratinocyte fluorescence lifetime differences—from endogenous fluorophores—between young (20 to 35 years old) and old (>60 years old) volunteers in photo-damaged forearm skin.[29]

We observed a significant increase in the average fluorescence lifetime of keratinocytes in the SB epidermal layer, between 20 to 29 and 30 to 39 year old subjects, in solar-protected skin [Fig. 5(a)]. However, the tendency reversed as the average fluorescence lifetime of 40 to 49 and 50 to 59 year olds was comparable to 20 to 29 year old subjects [Fig. 5(a)]. Differences in our results compared to Benati et al.[29] may be attributed to methodology, as our subjects had a maximum age of 59 years old, as opposed to a minimum of 60 years old in Benati's study.

To our knowledge, this is the first study comparing solar-exposed and solar-protected skin across various age groups to examine photo-damage associated changes in the redox state of the epidermis. We demonstrate that solar-exposed forearm skin has a lower average lifetime compared to the solar-protected side (Figs. 4 and 5). This result corresponds to a lower short and long lifetime, along with a higher proportion of the short lifetime component (Fig. 6). Benati et al. suggest that the increase in the fluorescence lifetime of solar-exposed skin with age is likely due to an increase in the proportion of melanocytes within the epidermis.[29]

The τ_1, τ_2 and α_1 parameters of the solar-exposed and solar-protected SG (Figs. 5 and 6), while significantly different, are still comparable to keratinocytes and not melanocytes.[30] As a result, the lifetime differences observed between solar-exposed and solar-protected SG may be due to contrasting redox states within the keratinocytes. As α_1 is elevated in the solar-exposed

SG, this suggests a greater proportion of free[1] NAD(P)H within these cells. As the spectra and lifetimes of NADH and NADPH overlap,[1] it is difficult to ascertain which, or if both of these metabolic compounds are elevated relative to their α_2 protein-bound modalities. Nevertheless, as photo-damage is associated with greater oxidative stress within the viable epidermis,[31] the natural antioxidant NADPH may be elevated in solar-exposed skin—relative to solar-protected skin—to counteract ROS-induced damage.

In the SB, the τ_1, τ_2 and α_1 parameters of solar-exposed skin [Fig. 6(b)] are comparable to melanocytes, whereas solar-protected skin appears to resemble keratinocytes.[30] As the solar-exposed forearm skin is more susceptible to photo-damage, elevated melanin production in response to photo-damage[32] would appear to explain the fluorescence lifetime differences observed in our study.

Acute photo-damaged skin is reported to have impaired barrier function relative to undamaged skin,[3,4] which may lead to greater penetration of foreign agents into the viable layers of the skin. Intravital stains such as indocyanine green and fluorescein have been used to fluorescently label epidermal-dermal cells for imaging by confocal and multiphoton laser scanning microscopy.[33,34] This intravital staining is typically administered via a subdermal injection of the fluorescent dyes into *in vivo* skin. Our data shows that there was no difference in the staining of the viable epidermis between solar-exposed and solar-protected forearm skin, of 20 to 29 and 50 to 59 year old subjects, after the topical application of fluorescent compounds acriflavine and/or 6-CF (Fig. 7). This suggests that there was inadequate penetration of these two stains from the aqueous solutions applied to the skin for both normal and chronic photo-damaged (solar-exposed) skin.

In conclusion, MPT-FLIM is an effective noninvasive optical technique to assess both intrinsic aging and photo-aging within *in vivo* human skin.

Acknowledgments

This work was supported by the National Health & Medical Research Council of Australia, the Cancer Council Queensland and the Cancer Council South Australia.

References

1. M. S. Roberts et al., "Non-invasive imaging of skin physiology and percutaneous penetration using fluorescence spectral and lifetime imaging with multiphoton and confocal microscopy," *Eur. J. Pharm. Biopharm.* **77**(3), 469–488 (2011).
2. L. Baillie et al., "Strategies for assessing the degree of photodamage to skin: a systematic review of the literature," *Br. J. Dermatol.* **165**(4), 735–742 (2011).
3. C. Gelis et al., "Modifications of *in vitro* skin penetration under solar irradiation: evaluation on flow-through diffusion cells," *Photochem. Photobiol.* **75**(6), 598–604 (2002).
4. W. M. Holleran et al., "Structural and biochemical basis for the UVB-induced alterations in epidermal barrier function," *Photodermatol. Photoimmunol. Photomed.* **13**(4), 117–128 (1997).
5. G. J. Fisher et al., "Pathophysiology of premature skin aging induced by ultraviolet light," *N. Engl. J. Med.* **337**(20), 1419–1429 (1997).
6. J. H. Chung et al., "Modulation of skin collagen metabolism in aged and photoaged human skin *in vivo*," *J. Invest. Dermatol.* **117**(5), 1218–1224 (2001).
7. M. Y. Berezin and S. Achilefu, "Fluorescence lifetime measurements and biological imaging," *Chem. Rev.* **110**(5), 2641–2684 (2010).
8. K. Konig, "Clinical multiphoton tomography," *J. Biophoton.* **1**(1), 13–23 (2008).
9. S.-J. Lin et al., "Evaluating cutaneous photoaging by use of multiphoton fluorescence and second-harmonic generation microscopy," *Opt. Lett.* **30**(17), 2275–2277 (2005).
10. K. Sugata et al., "Evaluation of photoaging in facial skin by multiphoton laser scanning microscopy," *Skin Res. Technol.* **17**(1), 1–3 (2011).
11. S. Puschmann et al., "Approach to quantify human dermal skin aging using multiphoton laser scanning microscopy," *J. Biomed. Opt.* **17**(3), 036005 (2012).
12. M. J. Koehler et al., "*In vivo* measurement of the human epidermal thickness in different localizations by multiphoton laser tomography," *Skin Res. Technol.* **16**(3), 259–264 (2010).
13. M. J. Koehler et al., "Keratinocyte morphology of human skin evaluated by *in vivo* multiphoton laser tomography," *Skin Res. Technol.* **17**(4), 479–486 (2011).
14. T. A. Robertson, W. Y. Sanchez, and M. S. Roberts, "Are commercially available nanoparticles safe when applied to the skin?," *J. Biomed. Nanotechnol.* **6**(5), 452–468 (2010).
15. M. Ichihashi et al.,"UV-induced skin damage," *Toxicology* **189**(1–2), 21–39 (2003).
16. E. J. Kim et al., "UV decreases the synthesis of free fatty acids and triglycerides in the epidermis of human skin *in vivo*, contributing to development of skin photoaging," *J. Dermatol. Sci.* **57**(1), 19–26 (2010).
17. H. C. Ishikawa-Ankerhold, R. Ankerhold, and G. P. C. Drummen, "Advanced fluorescence microscopy techniques—FRAP, FLIP, FLAP, FRET and FLIM," *Molecules* **17**(4), 4047–4132, Molecular Diversity Preservation International (2012).
18. W. Y. Sanchez et al., "Analysis of the metabolic deterioration of *ex vivo* skin from ischemic necrosis through the imaging of intracellular NAD(P)H by multiphoton tomography and fluorescence lifetime imaging microscopy," *J. Biomed. Opt.* **15**(4), 046008 (2010).
19. H.-W. Wang et al., "Differentiation of apoptosis from necrosis by dynamic changes of reduced nicotinamide adenine dinucleotide fluorescence lifetime in live cells," *J. Biomed. Opt.* **13**(5), 054011 (2008).
20. M. C. Skala et al., "*In vivo* multiphoton fluorescence lifetime imaging of protein-bound and free nicotinamide adenine dinucleotide in normal and precancerous epithelia," *J. Biomed. Opt.* **12**(2), 024014 (2007).
21. S. J. Lin and L. Guarente, "Nicotinamide adenine dinucleotide, a metabolic regulator of transcription, longevity and disease," *Curr. Opin. Cell Biol.* **15**(2), 241–246 (2003).
22. J. M. Levitt et al., "Diagnostic cellular organization features extracted from autofluorescence images," *Opt. Lett.* **32**(22), 3305–3307 (2007).
23. J. Liang et al., "Study the oxidative injury of yeast cells by NADH autofluorescence," *Spectrochim. Acta A Mol. Biomol. Spectrosc.* **67**(2), 355–359 (2007).
24. M. El-Domyati et al., "Intrinsic aging vs. photoaging: a comparative histopathological, immunohistochemical, and ultrastructural study of skin," *Exp. Dermatol.* **11**(5), 398–405 (2002).
25. E. T. Obi-Tabot et al., "Changes in hepatocyte NADH fluorescence during prolonged hypoxia," *J. Surg. Res.* **55**(6), 575–580 (1993).
26. M. J. Koehler et al., "*In vivo* assessment of human skin aging by multiphoton laser scanning tomography," *Opt. Lett.* **31**(19), 2879–2881 (2006).
27. M. J. Koehler et al., "Intrinsic, solar and sunbed-induced skin aging measured *in vivo* by multiphoton laser tomography and biophysical methods," *Skin Res. Technol.* **15**(3), 357–363 (2009).
28. M. Wlaschek et al., "Solar UV irradiation and dermal photoaging," *J. Photochem. Photobiol. B-Biol.* **63**(1–3), 41–51 (2001).
29. E. Benati et al., "Quantitative evaluation of healthy epidermis by means of multiphoton microscopy and fluorescence lifetime imaging microscopy," *Skin Res. Technol.* **17**(3), 295–303 (2011).
30. E. Dimitrow et al., "Spectral fluorescence lifetime detection and selective melanin imaging by multiphoton laser tomography for melanoma diagnosis," *Exp. Dermatol.* **18**(6), 509–515 (2009).
31. L. Rittié and G. J. Fisher, "UV-light-induced signal cascades and skin aging," *Ageing Res. Rev.* **1**(4), 705–720 (2002).
32. L. Marrot and J.-R. Meunier, "Skin DNA photodamage and its biological consequences," *J. Am. Acad. Dermatol.* **58**(5), S139–S148 (2008).
33. L. D. Swindle et al., "View of normal human skin *in vivo* as observed using fluorescent fiber-optic confocal microscopic imaging," *J. Invest. Dermatol.* **121**(4), 706–712 (2003).
34. C. Jonak et al., "Intradermal indocyanine green for *in vivo* fluorescence laser scanning microscopy of human skin: a pilot study," *PLoS ONE* **6**(8), e23972 (2011).